High-Frequency Fluctuation Intensity as a Predictor of Post-Stenotic Dilatation in Swine

Bo-Wen Lin, Pao-Yen Lin, Yao-Hsiang Shih, Cheng-Lin Wu, Yeng-Ting Wu, and Meei Jyh Jiang

Abstract*—*Objective: **To identify the turbulent components of blood flow facilitating aortic lumen dilatation in a post-stenotic dilatation (PSD) porcine model.** ***Methods:*** **The porcine abdominal aorta (AA) was moderately coarctated to induce overt flow turbulence in the downstream region and to lead to dilatation in time periods between four and twelve weeks. We propose a new metric, fluctuation intensity (FI), to quantify turbulent fluctuations of pulsatile aortic flow measured within twenty minutes post-coarctation. Lumen perimeter ratio (LPR) of the distal-to-suprarenal AA was used to assess the degree of PSD. Using k-means clustering analysis, we first divided FI frequency spectrum into low- and high-frequency fluctuation intensity (LFFI and HFFI), and subsequently grouped animals with coarctation. Receiver operating characteristic (ROC) analysis was performed to evaluate the ability of the proposed metric to predict PSD.** ***Results:*** **The frequency band of the FI spectrum in facilitating aortic lumen dilatation was identified to be 40∼200 Hz. Using sham group as the reference, pigs receiving coarctation were clustered into two groups with (group A) and without (group B) increases in HFFI values. Coarctation significantly increased LPR values in group A, but not in group B. Moreover, group A exhibited a high probability density distribution on severe elastic fiber fragmentation. ROC analysis indicated HFFI to be capable of predicting PSD with excellent sensitivity and specificity.** ***Conclusion:*** **High-intensity, high-frequency components of blood flow fluctuations induced by moderate coarctation promote elastic lamella degradation and aortic lumen dilatation.** ***Significance:*** **HFFI application in flowmeter programs may provide a useful predictor of PSD.**

***Index Terms*—Post-stenotic dilatation, high-frequency fluctuation intensity, elastic fiber fragmentation, k-means clustering, support vector machine, fast Fourier transform.**

I. Introduction

PERSISTENT and partial narrowing of an artery can alter the profile of blood flow and cause the downstream arterial segment to dilate. This dilated remodeling of the downstream artery is called post-stenotic dilatation (PSD) [1]. PSD is closely associated with a few cardiovascular diseases, such as ascending aortomegaly with severe aortic valve stenosis [2], [3], thoracic aortic aneurysm distal to aortic coarctation, subclavian arterial enlargement with thoracic outlet syndrome consequent to cervical rib compression. Taking aortic valve stenosis as an example, the heart-ejected bloodstream passing the narrowed valve orifice produces high velocity and turbulent flow which mainly impacts on the middle ascending aorta. Under chronic hemodynamic insult, the structural integrity of the aortic wall is compromised with decreased wall strength, and aortomegaly at the middle ascending aorta develops thereafter [2]. Accordingly, flow turbulence downstream of stenosis plays a determinant role in the development of PSD [3].

The development of PSD, based on empirical clinical observation, relies on the presence of flow disturbance sufficient to produce an audible bruit and a palpable thrill. Moderate stenosis produces prominent turbulence, i.e., bruit and thrill, is effective in eliciting PSD, whereas very tight or mild stenosis is usually ineffective [1], [4]. Experimental evidence also suggests turbulence to be a major cause of PSD [1], [4], [5]. To examine the role of turbulence in vivo in the development of aortic PSD, we established a coarctation-induced degenerative abdominal aortic aneurysm (AAA) porcine model [6] (Fig. 1(a)). To achieve moderate stenosis of the porcine aorta, we chose pulsatility index (PI) [7], [8], as the quantitative parameter of coarctation severity. PI reduction to one-third of the original value was found to accompany a pronounced turbulence in the abdominal aortic region distal to coarctation and hence was selected to indicate moderate stenosis. PSD was detected in the majority, but not all, of the pigs undergoing aortic coarctation up to 12 weeks. These results suggested that the exact characteristic of turbulent flow promoting aortic PSD remains to be pinpointed.

Manuscript received 1 January 2022; revised 30 May 2022 and 26 July 2022; accepted 7 September 2022. Date of publication 15 September 2022; date of current version 20 February 2023. The work of Bo-Wen Lin was supported by the Ministry of Science and Technology of Taiwan under Grant MOST106-2221-E-344-002. The work of Pao-Yen Lin was supported by the Funding of National Cheng Kung University Hospital under Grant NCKUH-10602019 and Grant NCKUH-10704007. The work of Meei Jyh Jiang was supported by the Ministry of Science and Technology of Taiwan under Grant NSC98-2320-B-006-025-MY3 and Grant NSC102-2320-B-006-045. *(Corresponding authors: Pao-Yen Lin; Meei Jyh Jiang.)*

Bo-Wen Lin is with the Department of Aircraft Engineering, Air Force Institute of Technology, Taiwan.

Pao-Yen Lin is with the Department of Surgery, Division of Cardiovascular Surgery, National Cheng Kung University Hospital, Tainan 70403, Taiwan, and also with the Department of Surgery, College of Medicine, Tainan 701401, Taiwan (e-mail: pylin@mail.ncku.edu.tw).

Yao-Hsiang Shih is with the Department of Anatomy, School of Medicine, College of Medicine, Kaohsiung Medical University, Taiwan.

Cheng-Lin Wu is with the Department of Pathology, National Cheng Kung University Hospital, Taiwan.

Yeng-Ting Wu is with the Department of Cell Biology and Anatomy, College of Medicine, National Cheng Kung University, Taiwan.

Meei Jyh Jiang is with the Department of Cell Biology and Anatomy, College of Medicine, National Cheng Kung University, Tainan 701401, Taiwan (e-mail: mjiang@ncku.edu.tw).

This article has supplementary downloadable material available at https://doi.org/10.1109/TBME.2022.3207060, provided by the authors.

Digital Object Identifier 10.1109/TBME.2022.3207060

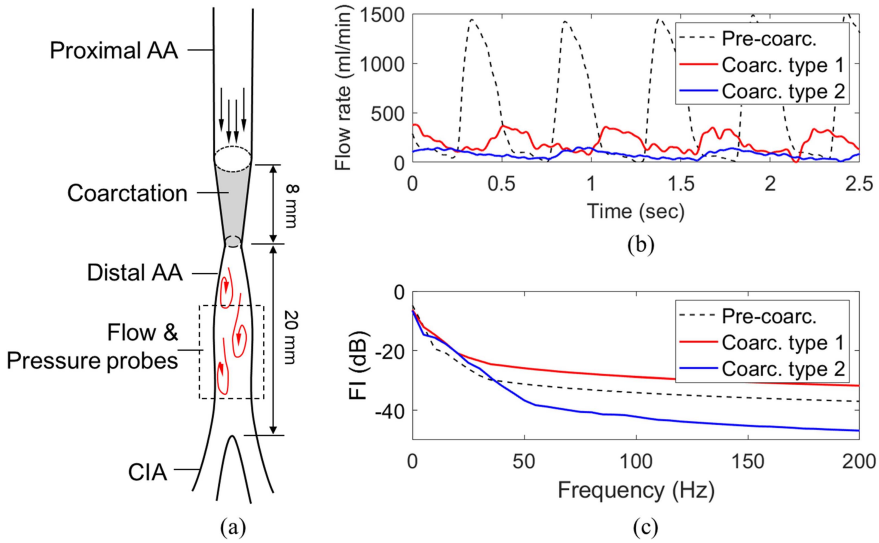

Fig. 1. (a) Coarctation-induced aortic lumen dilatation porcine model. The pronounced turbulent flow was generated in the aortic segment distal to coarctation. (b) Representative waveforms of measured blood flow rates in the distal abdominal aorta (AA) region before and after coarctation. (c) The spectrum of fluctuation intensity (FI) was calculated from the measured blood flow rates. After coarctation, different types of turbulent waveform correspond to different degrees of fluctuation intensity. AA: abdominal aorta; CIA: common iliac artery; FI: fluctuation intensity; dB: decibel.

Turbulence is chaotic fluid motion characterized by rapid fluctuations in its flow dynamic properties, e.g., flow velocity, flow rate, and wall shear stress (WSS). Randomly fluctuating flow dynamics usually cause irregular wall motion during cardiac cycles, and that may accelerate the degenerative process of the arterial wall. Pulsatile flow passing through the stenotic segment also enhances the flow dynamic fluctuation at the downstream arterial segment. In our porcine model, we found different types of turbulent flow waveforms at the distal aortic regions following coarctation (Fig. 1(b)) even though PI was reduced to one-third inherent levels and turbulence was visualized with duplex ultrasound. To identify the turbulent components of blood flow contributing to aortic dilatation, we used the fast Fourier Transform (FFT) method to analyze the measured blood flow rates and introduced a new metric for quantifying the pulsatile and turbulent flow-induced fluctuation intensity. In the present work, we aim i) to propose a metric to quantify the intensity of flow fluctuations from perivascular flow probes; ii) to identify the frequency bands of flow fluctuation intensity relevant in facilitating aortic lumen dilatation; iii) to assess the ability of the proposed metric as a predictor of PSD.

II. Methods

An overview of the methodology used in this study is shown in Fig. 2. The analysis of the results was conducted in five parts: i) correlation analysis was performed between the two sets of data, fluctuation intensity (FI) and lumen perimeter ratio (LPR), to explore the correlation between fluctuation intensity and aortic lumen dilatation; ii) k-means cluster analysis was employed to divide the FI frequency spectrum into two bands, low-frequency fluctuation intensity (LFFI) and high-frequency fluctuation intensity (HFFI), based on the results of correlation analysis; iii) animals of the experimental group (N = 20) were clustered into subgroups A and B using k-means cluster analysis; iv) statistical analysis was conducted to summarize the differences among the groups A, B, and sham; v) receiver operating characteristic (ROC) analysis was performed to evaluate the ability of LFFI and/or HFFI to predict for PSD formation.

A. Coarctation-Induced Aortic Lumen Dilatation Porcine Model

Twenty-eight Taiwanese Lanyu mini pigs of both genders, provided by Taitung Animal Propagation Station of the Taiwan Livestock Research Institute, were randomly divided into four groups: three experimental groups (6–9 pigs/group) undergoing aortic coarctation for 4 weeks (4w), 8 weeks (8w), and 12 weeks (12w) and sham groups (n = 8) as the control. The whole study conforms to the *Guide for the Care and Use of Laboratory Animals* published by the National Institute of Health (U. S. A.) and the experimental procedures were approved by the Institutional Animal Care and Use Committee (IACUC no. 98101, 102257).

Mini pigs were first sedated by intramuscular injection of a mixture of Zoletil 50 (10 mL), Rompun (5 mL), and atropine (1 mL) at pigs' posterior neck or gluteal region. Intravenous fluid infusion routes were established through the postauricular veins. During surgery, isoflurane (2% of the tidal volume) was continuously given via endotracheal tubing to maintain general anesthesia. Coarctation was conducted by encircling an 8 mm-wide expanded polytetrafluoroethylene (ePTFE) Teflon strip around the infrarenal abdominal aorta (AA) segment, approximately 2 cm proximal to the aortic bifurcation, to form a funnel-shaped pathway with a nonconstrictive inlet and a constrictive outlet (Fig. 1(a)) as previously described [6]. The extent of outlet constriction was adjusted by tightening or loosening the lower edge of the ePTFE strip according to PI values. A transit time flowmeter system (MediStim BF 2004; MediStim ASA, Oslo, Norway; 6 and 8 mm flow probes) was used to simultaneously monitor flow, pressure, and pulsatility index (PI, calculated from

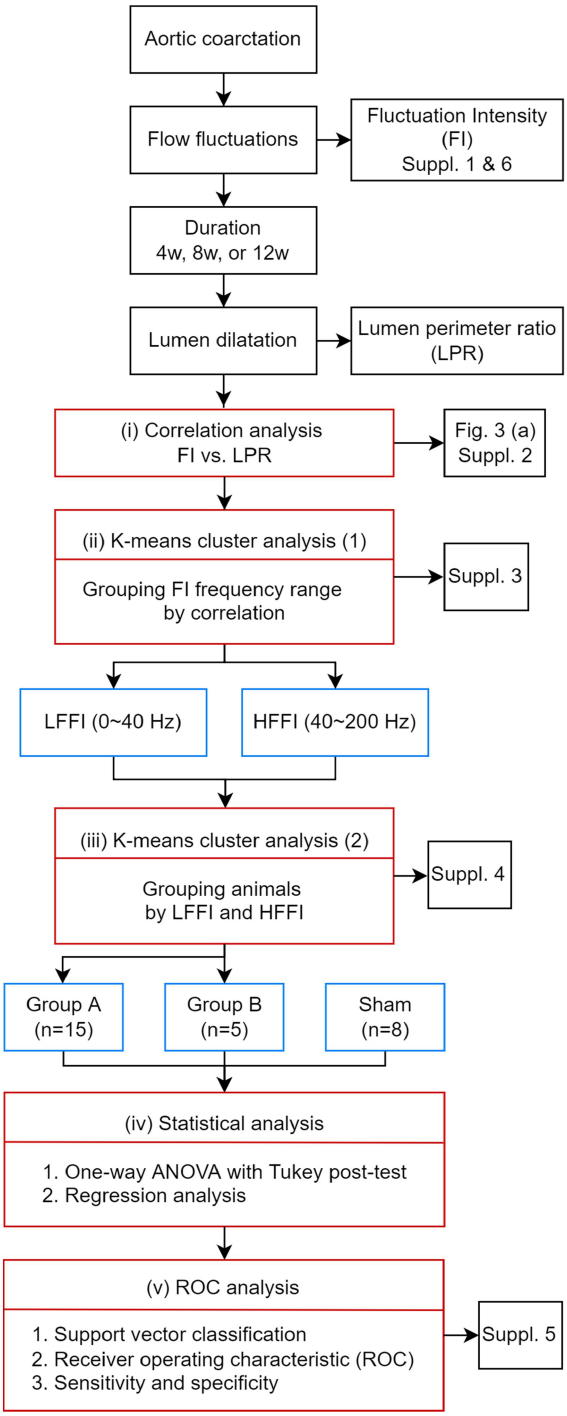

Fig. 2. Schematic illustration of the experimental/analytical procedure and methodology used in this study. The analysis framework mainly consists of five parts: (i) correlation analysis was performed between the two sets of data, FI and LPR, to explore the correlation between fluctuation intensity and aortic lumen dilatation; (ii) k-means cluster analysis was employed to divide the FI frequency spectrum into two bands, LFFI and HFFI, based on the results of correlation analysis; (iii) animals of the experimental group (N = 20) were clustered into subgroups A and B using k-means cluster analysis; (iv) statistical analysis was conducted to summarize the differences among the groups A, B, and sham; (v) ROC analysis was performed to evaluate the ability of LFFI and/or HFFI to predict for post-stenotic dilatation. FI: fluctuation intensity; LPR: lumen perimeter ratio; LFFI: low-frequency fluctuation intensity; HFFI: high-frequency fluctuation intensity; ANOVA: analysis of variance; ROC: receiver operating characteristic.

(maximal flow rate – minimal flow rate)/mean flow rate) [8] at the regions proximal and distal to coarctation both during the operation and prior to sacrifice [6]. Markedly disturbed waveforms with irregular margins in the distal AA were displayed by the flowmeter system as PI was greatly reduced. Duplex ultrasound scanning was also conducted to confirm turbulence development. When PI was reduced to one-third of the original value, a pronounced mosaic flow pattern was shown by ultrasound scanning images with decreased peak systolic flow and increased reverse flow in Doppler spectral analysis. Hence, we set PI reduction to one-third of the original value as the guide for moderate stenosis. The monitored flow waveforms were exported through the system's built-in function. Digital signals were obtained using GetData Graph Digitizer version 2.26. Animals were sacrificed with an intravenous injection of KCl (2 mmol/kg body weight).

B. Histological Examination of the Distal Abdominal Aorta

To examine the perimeter and the distribution of the elastic lamellae in the dilatation-prone distal AA segment, we performed Verhoeff Van Gieson staining. Paraffin sections (4 μm thick) were deparaffinized, rehydrated, and stained according to the manufacturer's instructions. The lumen perimeter of the distal AA segment was measured in paraffin-embedded sections with Image J software and values were further normalized with the lumen perimeter of the suprarenal AA segment. The degree of the elastic fiber fragmentation and/or loss (EFF) was evaluated blindly by a pathologist according to a previously reported consensus grading scheme [9]. Briefly, the extent of EFF was examined under 100x magnification in four sections per aorta with 80 μm intervals (240 μm between the 1st and 4th sections) and was classified into mild ($< 10\%$), moderate ($10\sim30\%$), or severe ($>30\%$).

C. Metric of Fluctuation Intensity

The intensity of flow turbulence was represented by the root mean square value of the high-frequency fluctuating components of flow velocity using Fourier analysis applied to in vivo study [10]. Analogously, fluctuation intensity (FI) is calculated from blood flow rate measured within twenty minutes post-coarctation and given by the root mean square value of the normalized amplitude of the Fourier components:

$$\mathrm{FI}_{(a\sim b\ \mathrm{Hz})} = \sqrt{\frac{1}{m}\sum_{f=a}^{b}\left(\frac{A(f)}{A(f)_{HR}}\right)^2}, \qquad (1)$$

in which the frequency-dependent value $A(f)$ is the amplitude of the Fourier components of blood flow rate, the reference value $A(f)_{HR}$ is the amplitude at heart rate frequency, and m is the sample size of calculations carried out for a range of frequencies $f = a$ to b. Briefly, the monitored blood flow rate in the distal AA segment (Fig. 1(b)) was transformed into the frequency domain using the fast Fourier transform (FFT) method. Each component of the normalized FFT amplitude (i.e., A/A_{HR}) was squared and summed over a specific frequency range, and the

square root was calculated. Frequencies above 200 Hz were not considered because the data was collected with a sampling rate of 500 Hz, giving a Nyquist frequency of 250 Hz (i.e., one-half of the sampling rate). To capture turbulence spectra, the FFT was performed with a rectangular window from 2500 points signal (equivalent to a time span of 5 s) without post-treatment using custom software MATLAB (Version R2019a). Signals of two or three 5-s time span were analyzed for each aorta. The reliability of the FI index was validated in the reproducibility test (Supplement 1). In addition, because the flow spectrum presents a span of several orders of magnitude, decibel notation is used to express FI values as follows:

$$\mathrm{FI}\ (\mathrm{dB}) = 10 \log_{10} (\mathrm{FI}) . \tag{2}$$

Eqs. (1) and (2) give the relative intensity in decibels as a simple metric in quantifying the intensity of blood flow fluctuation (Fig. 1(c)). FI = 0 dB indicates that the fluctuation intensity is equal to the reference value; FI < 0 dB means that the fluctuation intensity is smaller than the reference value, whereas FI > 0 dB means the opposite.

D. Data Processing and Cluster Analysis

The objectives of data processing are twofold. First, to divide the FI frequency spectrum into LFFI and HFFI corresponding to the intensity of pulsatile fluctuations and turbulent fluctuations [11], respectively. Secondly, to categorize experimental animals into groups based on coarctation-induced changes in LFFI and HFFI. To these ends, cluster analysis was applied.

Cluster analysis is an unsupervised machine learning technique [12] that performs its tasks without prior knowledge of the group definition. Among partition-based clustering algorithms, k-means clustering is the simplest and most commonly applied [12]. The principle of the k-means clustering is to divide an N-dimensional population into k sets by the criterion of minimizing the within-cluster variance [13]. Because the choice of k-value directly affects the clustering results [14], extensive cluster validity indices are usually compared to evaluate the clustering performance [15]. In this study, four cluster validity indices, namely rule of thumb, Davies-Bouldin index, elbow method, and silhouette coefficient [14], [15], [16], were calculated to select the optimal k-value, as shown in supplementary materials (supplemental results can be found online at https://doi.org/10.6084/m9.figshare.16767220). The cluster analysis was performed in Python version 2.7 with the module of scikit-learn version 1.0 [17].

E. Hemodynamic Parameters

The ratio of mean arterial pressure to mean flow rate detected at the distal AA was calculated to represent the overall resistance of the vessels distal to this location. The stroke volume in the distal AA (SV_{DAA}) was obtained from the mean flow rate divided by the heart rate.

F. Statistical Analysis

Data were expressed as mean ± standard deviation; n indicates the number of pigs. *P* values were evaluated by one-way ANOVA with Tukey post-test, and $P < 0.05$ was considered statistically significant. To examine the correlation between two parameters, the variance of the correlation coefficient (R^2) was obtained through linear or nonlinear regression analysis. Statistical analysis was conducted using GraphPad Prism version 7 (GraphPad Software, San Diego, California, USA).

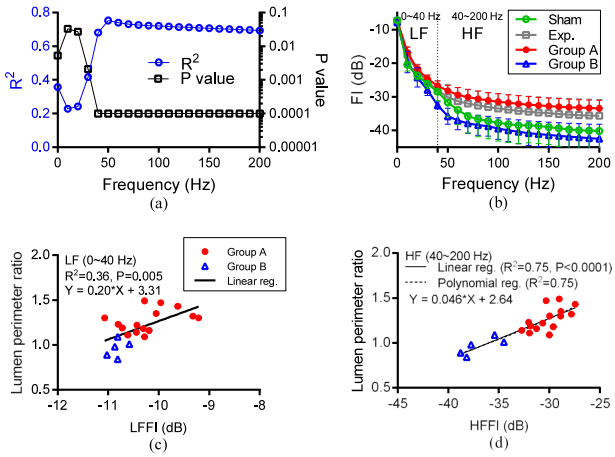

Fig. 3. Fluctuation intensity (FI) increases correlate with coarctation-induced lumen perimeter dilatation. (a) The correlation between FI values and lumen perimeter ratio indicates a higher correlation for FI values at frequencies over 40 Hz. (b) FI values for the frequency spectrum of 0–200 Hz with 10 Hz intervals were calculated for the sham group, experimental group, and subgroups A and B of the experimental group. High-frequency FI values of group A, but not group B, appeared greater than those of the sham group. (c)–(d) Lumen perimeter ratio of groups A and B exhibited weak and moderate correlation with FI values obtained from low-frequency (c) and high-frequency (d) ranges, respectively. Values were expressed as mean ± SD. R^2: the square of the Pearson correlation coefficient; FI: fluctuation intensity; LF: low-frequency; HF: high-frequency.

G. Receiver Operating Characteristic Analysis

ROC analysis [18] was performed to evaluate the ability of LFFI and/or HFFI as a predictor for detecting sham (control), group A (PSD), and group B (stenosis without PSD). Since this is a multi-class classification problem, the algorithm of support vector classification [19] with a linear kernel in conjunction with the one-vs.-rest method [20] was adopted to handle the task. Detection ability was represented by indices of the area under the ROC curve (AUC), sensitivity, and specificity as summarized in Table S5. The optimal values of sensitivity and specificity for each ROC curve were selected based on the Youden index [21]. The ROC analysis was achieved by machine learning algorithms in Python with the module of scikit-learn [17].

III. Results

A. Correlation and Frequency Bands

The strength of correlation between FI values and LPR was assessed by correlation and regression analysis [22]. FI values were positively correlated with LPR with those at frequencies below 40 Hz showing weak correlation and those over 40 Hz exhibiting a stronger correlation (Fig. 3(a) and Supplement 2). Based on the results of correlation analysis, the relevant frequency bands of FI facilitating aortic lumen dilatation were identified using

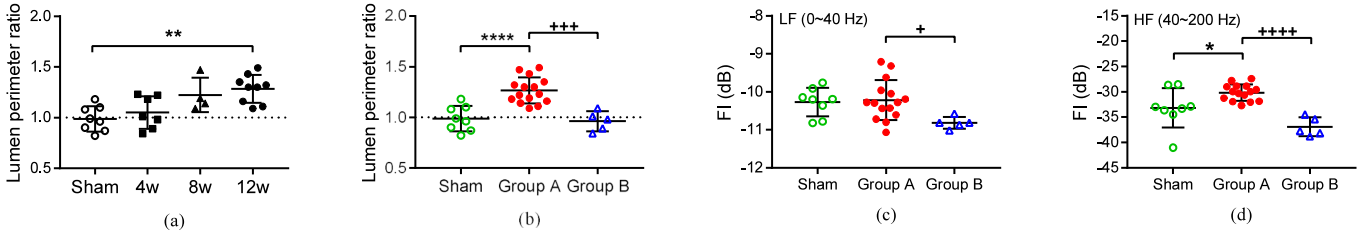

Fig. 4. Characterization of coarctation-induced turbulent flow and aortic lumen dilatation. Three experimental groups (4–12 pigs/group) underwent aortic coarctation for 4 weeks (4w), 8 weeks (8w), and 12 weeks (12w) with the sham group (N = 8) as the control. Using cluster analysis, the animals of the experimental group were clustered into subgroups A and B. (a) Lumen perimeter ratio of the distal-to-suprarenal abdominal aorta segment was shown in a time-dependent manner. After clustering, lumen perimeter ratio (b), low-frequency fluctuation intensity (c), and high-frequency fluctuation intensity (d) were compared among groups A, B, and sham. Values were expressed as mean ± SD, $^{*}<0.05$, $^{**}<0.01$, $^{****}<0.0001$ vs. sham group; $+<0.05$, $+++<0.001$, $++++<0.0001$ vs. Group B. LF: low-frequency; HF: high-frequency; dB: decibel.

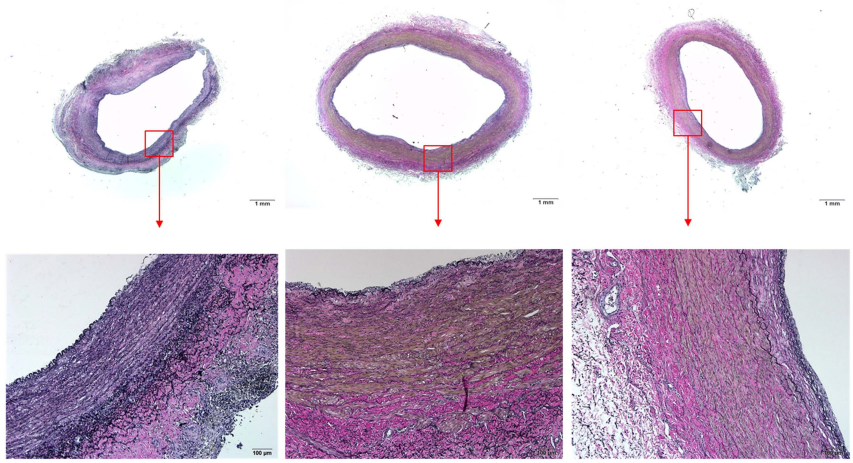

Fig. 5. Representative images of aortas with stained elastic lamellae in sham, group A, and group B pigs. Elastic lamellae were detected with Verhoeff Van Gieson staining. Representative images were shown for the sham group (a), group A (b), and group B (c). Scale bars: 1 mm for the upper panels; 100 μm for the lower panels.

k-means cluster analysis. As shown in Fig. 3(b) and Supplement 3, the FI frequency spectrum was divided into low-frequency (LF) and high-frequency (HF) bands corresponding to the frequency range of 0∼40 Hz and 40∼200 Hz, respectively. The linear regression analysis indicated a weak correlation between LFFI and LPR ($R^2 = 0.36$, Fig. 3(c)). In contrast, HFFI exhibited moderate correlation with LPR based on linear regression ($R^2 = 0.75$) and nonlinear regression ($R^2 = 0.75$, Fig. 3(d)).

B. Differences Between Study Groups

Aortic coarctation induced lumen dilatation of the distal AA in a time-dependent manner (Fig. 4(a)). At 12w, mini pigs undergoing AA coarctation exhibited marked increases in LPR, approximately 30%, compared to the sham group. It was, however, noted that some pigs exhibited negligible or non-significant aortic dilatation. Moderate aortic coarctation in our animal model [6] was performed based on pulsatility index [8] reduction to one-third of the inherent levels. Flow fluctuation analysis as indicated with FI showed that coarctation can induce flow fluctuations to different degrees and even with different patterns (Fig. 1(b) and (c)).

To better understand the impact of coarctation variation, k-means clustering was conducted to categorize experimental animals into groups A (N = 15) and B (N = 5). The detailed results of cluster analysis were presented in Supplement 4. The LPR of group A (1.27 ± 0.13) was significantly higher than that of the sham group (0.99 ± 0.12), whereas no difference was detected between group B (0.96 ± 0.10) and sham (Fig. 4(b)). Accordingly, group A and group B were classified as having PSD and stenosis without PSD, respectively.

When the fluctuation intensity of both frequency bands was analyzed, no difference was detected in LFFI of either group A (-10.22 ± 0.52 dB) or group B (-10.82 ± 0.16 dB) compared with the sham group (-10.27 ± 0.38 dB) (Fig. 4(c)). In contrast, the HFFI of group A (-30.16 ± 1.60 dB) was significantly higher than that of the sham group (-33.19 ± 3.89 dB) and group B (-36.92 ± 1.87 dB), whereas no difference was detected between group B and sham (Fig. 4(d)). These results implicate higher HFFI in PSD.

When we examined the elastic lamellae, compared with the sham group (Fig. 5(a)), degradation of elastic lamellae was prominent in group A (Fig. 5(b)), whereas marked fragmentation accompanied by less degradation was detected in group

TABLE I
THE BASIC INFORMATION OF THE MINI PIGS ANALYZED IN THIS STUDY

No	Group	Age (months)	Gender	Duration (weeks)	Weight (kg)	Lumen perimeter (mm)	Lumen perimeter ratio	FI (dB) (0-40 Hz)	FI (dB) (40-200 Hz)	Degree of EFF
54	A	6	F	4	NA	17.36	1.22	-10.43 ± 0.45	-30.65 ± 0.66	3
59	A	6	F	4	NA	14.07	1.23	-10.80 ± 0.14	-32.04 ± 2.81	2
65	A	15	F	12	NA	21.66	1.11	-10.61 ± 0.11	-31.96 ± 5.26	3
67	A	15	M	12	NA	19.28	1.35	-10.05 ± 0.67	-28.84 ± 1.24	3
68	A	15	F	12	NA	19.64	1.43	-9.62 ± 0.02	-27.42 ± 0.67	3
71	A	14	M	8	NA	21.20	1.47	-9.96 ± 0.08	-30.31 ± 2.49	3
76	A	9	F	4	41	18.00	1.18	-10.30 ± 0.05	-29.60 ± 1.14	2
78	A	10	M	8	50	18.50	1.19	-10.72 ± 0.12	-31.87 ± 0.33	2
84	A	11	M	8	56	17.00	1.09	-10.28 ± 0.66	-30.00 ± 0.70	2
86	A	11	F	8	53	18.10	1.14	-10.44 ± 0.03	-32.71 ± 0.98	3
90	A	11	M	12	67	18.60	1.30	-11.07 ± 0.10	-29.96 ± 0.07	2
95	A	15	M	12	72	17.36	1.32	-9.32 ± 0.37	-27.82 ± 0.65	NA
96	A	15	M	12	75	19.60	1.30	-9.21 ± 0.18	-28.88 ± 0.77	NA
98	A	15	F	12	63	16.83	1.16	-10.19 ± 0.40	-31.26 ± 3.98	3
99	A	15	M	12	70	19.42	1.49	-10.28 ± 0.13	-29.01 ± 0.08	3
55	B	7	F	4	NA	11.72	0.89	-11.02 ± 0.04	-38.79 ± 1.04	3
64	B	15	F	12	NA	16.63	1.09	-10.81 ± 0.27	-35.40 ± 2.10	3
80	B	9	F	4	45	14.70	1.01	-10.58 ± 0.14	-34.48 ± 2.64	2
81	B	9	M	4	44	12.70	0.84	-10.81 ± 0.04	-38.17 ± 3.66	3
83	B	9	M	4	52	14.40	0.98	-10.87 ± 0.04	-37.74 ± 1.68	1
66	Sham	15	M	12	NA	16.50	0.90	-10.15 ± 0.32	-41.03 ± 0.21	2
70	Sham	14	M	8	NA	11.91	0.82	-10.36 ± NA	-33.65 ± NA	2
77	Sham	10	F	8	54	16.20	1.18	-10.20 ± 0.23	-28.54 ± 0.79	2
82	Sham	9	M	4	44	14.20	1.08	-9.91 ± 0.06	-33.34 ± 0.26	2
85	Sham	9	M	4	46	16.10	1.10	-9.76 ± 0.07	-32.95 ± 0.36	2
87	Sham	11	M	8	57	14.70	0.99	-10.82 ± 0.10	-34.50 ± 0.29	2
88	Sham	11	F	8	57	14.90	0.96	-10.78 ± 0.11	-28.63 ± 0.22	2
89	Sham	12	F	12	58	15.50	0.87	-10.19 ± 0.13	-32.89 ± 0.16	1

The lumen perimeter of the distal abdominal aorta (AA) segment was measured in paraffin-embedded sections and values were normalized with the lumen perimeter of the suprarenal AA segment. Fluctuation intensity values (mean ± standard deviation) were calculated from low-frequency (0-40 Hz) and high-frequency (40-200 Hz) of flow rates measured within twenty minutes post-coarctation. Elastic fiber fragmentation/loss was graded as grade 1 (< 10%), grade 2 (10~30%), or grade 3 (> 30%). FI: Fluctuation intensity; dB: decibel; EFF: elastic fiber fragmentation/loss; NA: not available.

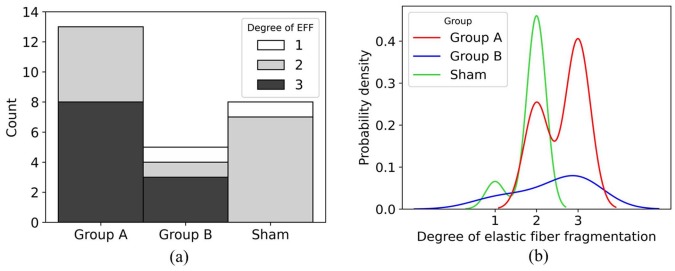

Fig. 6. The degree of elastic fiber fragmentation in groups A, B, and sham. Evaluation results were shown in animal count (a) and probability density distribution (b). The extent of elastic fiber fragmentation and/or loss was graded into grade 1 (<10%), grade 2 (10∼30%), or grade 3 (>30%). The probability density distribution was estimated using Gaussian kernels. EFF: elastic fiber fragmentation and/or loss.

B (Fig. 5(c)). As shown in Fig. 6, both groups A and B exhibit more severe (or grade 3) elastic fiber fragmentation and/or loss (EFF) than the sham group which mainly exhibits grade 2 EFF. The basic information of the twenty-eight mini pigs analyzed in this study, including age, gender, body weight, and duration of aortic coarctation, was listed in Table I with post-coarctation FI values and LPR as well as EFF at sacrifice.

C. Coarctation-Induced Changes in Hemodynamics

To determine the relationship between hemodynamics and aortic lumen dilatation, we measured hemodynamic parameters including flow rate and arterial pressure at the distal AA. AA coarctation caused marked decreases in mean arterial flow rate (MAF, Fig. 7(a)), pulse pressure (PP, Fig. 7(b)), but not for the mean arterial pressure (MAP, Fig. 7(c)) at the distal AA. At sacrifice, these parameters recovered mostly. We also calculated arterial resistance at the distal AA (R_{DAA}), presented as the ratio of MAP to MAF. Coarctation slightly increased the resistance at the distal AA, which recovered to near pre-coarctation levels at sacrifice in both groups A and B (Fig. 7(d)). No significant difference in heart rate (HR) was detected at surgery and sacrifice (Fig. 7(e)). When we calculated stroke volume at the distal AA (SV_{DAA}), coarctation caused immediate decreases in stroke

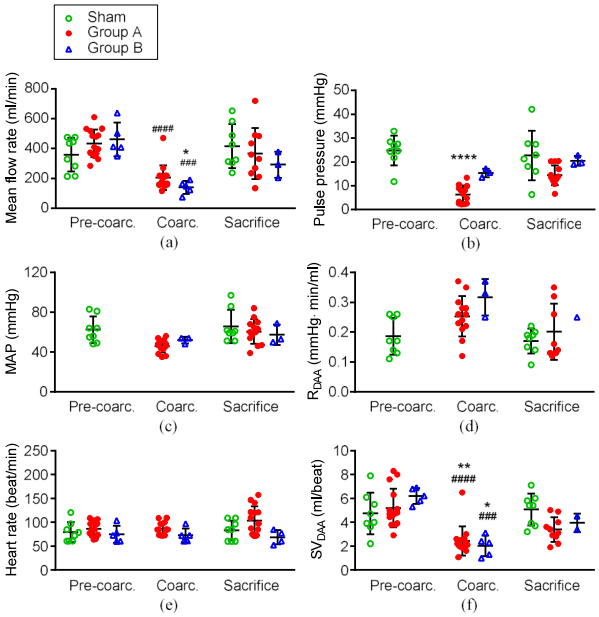

Fig. 7. Hemodynamic parameters following AA coarctation and before sacrifice. Mean blood flow rates (a) were measured in the distal AA (DAA) region before coarctation, after coarctation, and before sacrifice. Intravascular blood pressures were measured in the DAA following coarctation and before sacrifice. Pulse pressure (b), mean arterial pressure (c), and resistance (d) of the DAA were calculated. Heart rate (e) and stroke volume in the distal AA region (SV_{DAA}, f) were calculated for groups A, B, and sham before coarctation, after coarctation, and before sacrifice. Values were expressed as mean ± SD, $^{*}< 0.05$, $^{**}< 0.01$, $^{****}<0.0001$ vs. sham group; ###< 0.001, ####< 0.0001 vs. pre-coarctation. AA: abdominal aorta; DAA: distal abdominal aorta; MAP: mean arterial pressure; SV: stroke volume.

volume in both groups A and B, which slightly recovered at sacrifice (Fig. 7(f)). In summary, coarctation caused insignificant differences between groups A and B in hemodynamic parameters including MAF, PP, MAP, R_{DAA}, HR, and SV_{DAA}.

D. The Proposed Metric As a Predictor of PSD

As shown in Fig. 8, the probability density distributions of LFFI and HFFI were evaluated for all three groups. The distribution of all groups almost completely overlaps on LFFI (Fig. 8(a)). On the distribution of HFFI (Fig. 8(b)), group A and group B slightly overlap with each other, whereas sham partially overlaps with groups A and B. Therefore, the probability density distributions indicate the feasibility to predict PSD with HFFI.

The ability of LFFI and/or HFFI as a predictor for detecting sham (control), group A (PSD), and group B (stenosis without PSD) was evaluated by one-vs.-rest ROC analysis. As shown in Fig. 9, HFFI detected sham, group A, and group B with AUC of 0.38, 0.87, and 0.95, respectively. The Youden index provided the optimal values of sensitivity and specificity of 1.00 and 0.85 for detecting group A, 1.00 and 0.91 for group B, and 0.25 and 0.90 for sham. When combining LFFI and HFFI as a predictor (Fig. S5-2(a)), the sensitivity and specificity for group A remain the same as HFFI alone. In addition, LFFI (Fig. S5-2(b)) performed the worst of all three predictors with AUC of 0.39, 0.64, and 0.90 for detecting sham, group A, and group

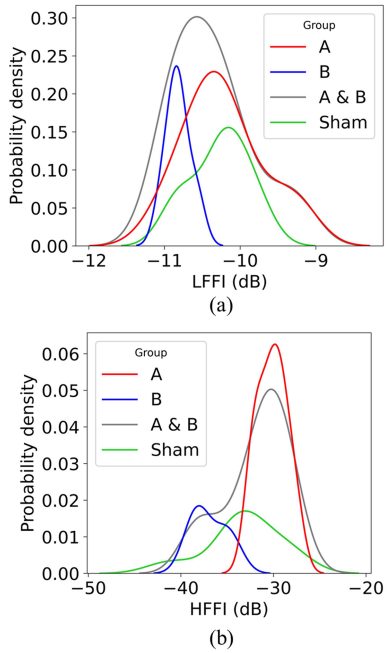

Fig. 8. The probability density distribution of LFFI (a) and HFFI (b) for groups A, B, and sham. Kernel-density estimates were obtained using Gaussian kernels. LFFI: low-frequency fluctuation intensity; HFFI: high-frequency fluctuation intensity; dB: decibel.

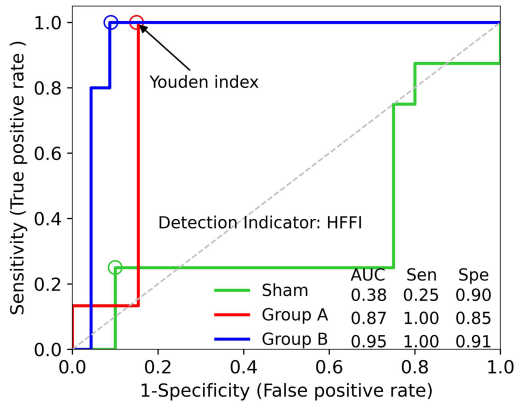

Fig. 9. Receiver operating characteristic (ROC) curves for prediction of sham (control), group A (PSD), and group B (stenosis without PSD) with indicator HFFI. The optimal values of sensitivity and specificity for each ROC curve, as indicated with circles, were selected based on the Youden index. AUC: area under ROC curve; HFFI: high-frequency fluctuation intensity; PSD: post-stenotic dilatation; Sen: sensitivity; Spe: specificity.

B, respectively. It was reported that an AUC value of 0.7 to 0.8 is acceptable and a value greater than 0.9 is outstanding for an indicator [23]. Therefore, HFFI can serve as a predictor of PSD.

IV. Discussion

In this study, we proposed the fluctuation intensity as a new metric in the blood flow field for quantifying pulsatile and turbulent fluctuations, referred to as low-frequency FI and high-frequency FI. We found that high-intensity, high-frequency

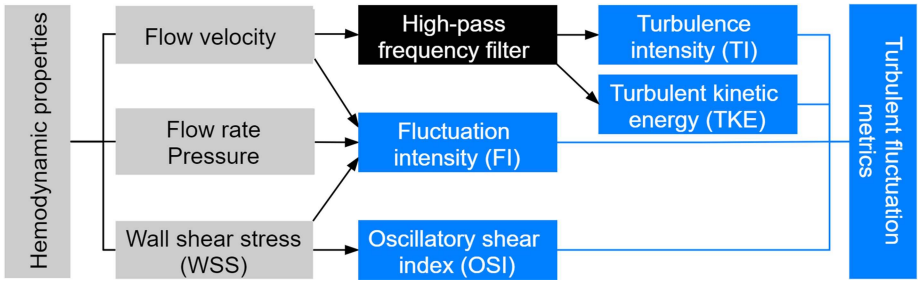

Fig. 10. Turbulent fluctuation-related metrics. Turbulent flow is characterized by significant fluctuations in flow velocity, flow rate, pressure, or wall shear stress caused by random and rapid fluid motion. The root mean square value of high-frequency, fluctuating components of the flow velocity is defined as turbulence intensity (TI). Oscillatory shear index (OSI) is a derivative of wall shear stress used to quantify instantaneous fluctuations. Fluctuation intensity (FI) proposed herein is a generalized form that can be applied to various pulsatile physiological waveforms. In particular, the high-frequency component of FI is equivalent to TI.

components of blood flow fluctuations induced by moderate coarctation promote elastic lamella degradation and aortic lumen dilatation. The frequency band of flow fluctuation intensity relevant in facilitating aortic lumen dilatation was identified to be 40∼200 Hz. Furthermore, the results of ROC analysis show that HFFI, i.e., $\mathrm{FI}_{(40\sim200\ \mathrm{Hz})}$, is capable of predicting PSD with excellent sensitivity and specificity.

PSD results from persistent moderate stenosis which produces chronic, high-intensity turbulence in the downstream arterial region. Early detection of moderate arterial stenosis, even asymptomatic, may prevent subsequent fatal events including aneurysm and dissection. Current first-line diagnostic methods to detect significant stenosis depend on physical examinations: auscultation and palpation [24]. While high-intensity post-stenotic turbulence occurs, an audible bruit or a palpable thrill can be detected in the downstream arterial region where PSD may develop [1]. Physical examinations are simple, non-invasive, low-cost, and convenient modalities for clinicians to diagnose stenotic arterial diseases and to follow up the progression. Such modalities are, however, experience-dependent and unable to quantify the degree of stenosis, and hence provide little help to predict disease progression and prevent adverse events. Taking carotid stenosis-induced audible bruit as an example, meta-analysis indicates that the pooled sensitivity and specificity are 0.53 and 0.83, respectively [24], [25]. Clearly, auscultation does not meet the reliability needed in the precise detection of stenosis. Given the fact that high-intensity turbulence is the prerequisite of eliciting PSD downstream, turbulence intensity is likely to play a key role in dilated aortic remodeling. An indicator capable of quantifying the intensity of stenotic-induced turbulence should prove useful in predicting PSD formation and further preventing late complications. Indeed, by analyzing our in vivo acquisition data, we found that high-intensity turbulent fluctuations identified by HFFI facilitate post-stenotic aortic dilatation and exhibit the feature of an excellent predictor of PSD. In this context, the frequency band of our HFFI (FI, 40∼200 Hz) corresponds to the intensity of flow instabilities (IFI) proposed by Mancini et al. [26]. Those authors introduced IFI as a metric to quantify the severity of carotid stenosis. They validated the frequency band for detecting pressure fluctuations induced by moderate stenosis to be 80∼200 Hz and proposed $\mathrm{IFI}_{(80\sim200\ \mathrm{Hz})}$ as an indicator for moderate stenosis. Our results are in good agreement with their in vitro results in terms of stenosis degree, frequency band, and fluctuation intensity metric.

Medial elastic lamellae are a major structural component to maintain arterial wall integrity [1]. Disruption or loss of medial elastic lamellae may lead to fatal arterial degenerative diseases including aortic aneurysm and dissection. Owing to the high similarity of the porcine cardiovascular system to that of humans both anatomically and physiologically [27], we examined the degree of medial EFF in the distal AA to evaluate the impact of coarctation-induced turbulent flow on the downstream aortic wall. Our semi-quantitative results (Fig. 6) that more severe EFF is detected in the PSD group (or group A) compared with the sham group fully substantiate this notion. On the other hand, severe EFF detected in group B (i.e., stenosis without PSD) exhibiting a percentage similar to that of group A appears contradicting with the lack of PSD. It is worth noting that severe EFF in this study is defined as over 30% damage of the medial elastic lamellae [9], but we have observed more pronounced elastic fiber loss in group A compared with group B as exemplified in Fig. 5((b) and (c)). There are limitations to our results on EFF analysis which was conducted semi-quantitatively because of enormous variation in quantified data between experiments. In addition, the lack of two blind and independent assessments may render the analysis less objective. Apart from quantitative analysis of medial EFF, investigations of changes in elastic fiber quality may provide further insight. As shown by a recent study, either quantitative or qualitative destruction of elastic fibers contributes to the degeneration of the aortic wall [28] and results in different degrees of aortic lumen dilatation. The relationship between the extent of EFF and aortic lumen dilatation warrants further studies.

The fluctuation intensity proposed in this study can be added to the list of turbulent fluctuation-related metrics including turbulence intensity (TI), turbulent kinetic energy, and oscillatory shear index (OSI) (Fig. 10). Over the years, the definition of turbulence and WSS has become confused and often misused in cardiovascular research [29]. Turbulence is a fluid phenomenon characterized by rapid fluctuations in fluid properties such as pressure, velocity, flow rate, and WSS. WSS, a function of the near-wall shear rate, is a widely used metric to link blood flow to

vascular biology [30], particularly on the endothelium [31]. Because WSS is insufficient to represent fluctuation characteristics of turbulence [29], OSI was introduced to reflect fluctuations in WSS [32]. TI, also referred to as turbulence level, is defined as the ratio of root mean square value of turbulent velocity fluctuations to a reference velocity value [33]. The FI proposed herein is a generalized metric of TI, in which the high-frequency component of FI is equivalent to TI (Fig. S6, see Supplement 6 for more details regarding the mathematical expression of FI and TI). In the current study, FI refers to the intensity of flow rate fluctuations. It should be noted that FI can be applied to other pulsatile physiological waveforms such as flow velocity, pressure, and WSS.

V. Conclusion

Results of this study identify HFFI as a predictor of aortic coarctation-induced lumen dilatation in swine. The moderate coarctation-induced high-intensity flow turbulence impacts the elastic lamellae to accelerate PSD. Furthermore, turbulence characterized by high-frequency fluctuations plays a key role to promote elastic lamella degradation and PSD of the aorta.

Acknowledgment

We thank Mr. Guan-Cheng Lin, Mr. Lin-Hsiang Yeh, and Mr. Yan-Shiang Yang for the assistance in conducting animal experiments, collecting data, and critically reviewing the manuscript. We thank the technical services provided by the "Bioimaging Core Facility of the National Core Facility for Biopharmaceuticals, Ministry of Science and Technology, Taiwan.

References

[1] P. Dobrin, "Poststenotic dilatation," *Surg. Gynecol. Obstet.*, vol. 172, no. 6, pp. 503–508, 1991.
[2] P. W. Fedak et al., "Clinical and pathophysiological implications of a bicuspid aortic valve," *Circulation*, vol. 106, no. 8, pp. 900–904, 2002.
[3] F. Robicsek et al., "Cause of ascending aortic dilatation in patients with bicuspid aortic valves: The final link," *Thorac. Cardiovasc. Surg.*, vol. 68, no. 4, pp. 277–280, Jun. 2020.
[4] M. R. Roach, "An experimental study of the production and time course of poststenotic dilatation in the femoral and carotid arteries of adult dogs," *Circ. Res.*, vol. 13, no. 6, pp. 537–551, 1963.
[5] M. Ojha et al., "Evidence of a possible link between poststenotic dilation and wall shear stress," *J. Vasc. Surg.*, vol. 11, no. 1, pp. 127–135, 1990.
[6] P. Y. Lin et al., "Coarctation-induced degenerative abdominal aortic aneurysm in a porcine model," *J. Vasc. Surg.*, vol. 57, no. 3, pp. 806–815, Mar. 2013.
[7] G. Beldi et al., "Transit time flow measurement: Experimental validation and comparison of three different systems," *Ann. Thorac. Surg.*, vol. 70, no. 1, pp. 212–217, 2000.
[8] M. Aleksic et al., "Pulsatility index determination by flowmeter measurement: A new indicator for vascular resistance ?," *Eur. Surg. Res.*, vol. 36, no. 6, pp. 345–349, 2004.
[9] M. K. Halushka et al., "Consensus statement on surgical pathology of the aorta from the society for cardiovascular pathology and the association for European cardiovascular pathology: II. Noninflammatory degenerative diseases—Nomenclature and diagnostic criteria," *Cardiovasc. Pathol.*, vol. 25, no. 3, pp. 247–257, 2016.
[10] P. D. Stein and H. N. Sabbah, "Turbulent blood flow in the ascending aorta of humans with normal and diseased aortic valves," *Circ. Res.*, vol. 39, no. 1, pp. 58–65, 1976.
[11] M. L. Thorne et al., "In vivo Doppler ultrasound quantification of turbulence intensity using a high-pass frequency filter method," *Ultrasound Med. Biol.*, vol. 36, no. 5, pp. 761–771, 2010.
[12] A. K. Jain et al., "Data clustering: A review," *ACM Comput. Surv.*, vol. 31, no. 3, pp. 264–323, 1999.
[13] J. MacQueen, "Some methods for classification and analysis of multivariate observations," in *Proc. 5th Berkeley Symp. Math. Statist. Prob.*, 1967, pp. 281–297.
[14] C. Yuan and H. Yang, "Research on K-value selection method of K-means clustering algorithm," *J*, vol. 2, no. 2, pp. 226–235, 2019.
[15] O. Arbelaitz et al., "An extensive comparative study of cluster validity indices," *Pattern Recognit.*, vol. 46, no. 1, pp. 243–256, 2013.
[16] T. M. Kodinariya and P. R. Makwana, "Review on determining number of cluster in k-means clustering," *Int. J.*, vol. 1, no. 6, pp. 90–95, 2013.
[17] F. Pedregosa et al., "Scikit-learn: Machine learning in Python," *J. Mach. Learn. Res.*, vol. 12, pp. 2825–2830, 2011.
[18] T. Fawcett, "An introduction to ROC analysis," *Pattern Recogn. Lett.*, vol. 27, no. 8, pp. 861–874, 2006.
[19] C.-C. Chang and C.-J. Lin, "LIBSVM: A library for support vector machines," *ACM Trans. Intell. Syst. Technol.*, vol. 2, no. 3, pp. 1–27, 2011.
[20] M. Aly, "Survey on multiclass classification methods," *Neural Netw.*, vol. 19, pp. 1–9, 2005.
[21] W. J. Youden, "Index for rating diagnostic tests," *Cancer*, vol. 3, no. 1, pp. 32–35, 1950.
[22] K. H. Zou et al., "Correlation and simple linear regression," *Radiology*, vol. 227, no. 3, pp. 617–628, 2003.
[23] J. N. Mandrekar, "Receiver operating characteristic curve in diagnostic test assessment," *J. Thorac. Oncol.*, vol. 5, no. 9, pp. 1315–1316, 2010.
[24] A. Elder et al., "How valuable is physical examination of the cardiovascular system?," *Br. Med. J.*, vol. 354, 2016, Art. no. i3309.
[25] P. McColgan et al., "Evaluation of the clinical utility of a carotid bruit," *Q. J. Med.*, vol. 105, no. 12, pp. 1171–1177, 2012.
[26] V. Mancini et al., "Computed poststenotic flow instabilities correlate phenotypically with vibrations measured using laser Doppler vibrometry: Perspectives for a promising in vivo device for early detection of moderate and severe carotid stenosis," *J. Biomech. Eng.*, vol. 142, no. 9, 2020, Art. no. 091007.
[27] A. C. Smith and M. M. Swindle, "Preparation of swine for the laboratory," *ILAR J.*, vol. 47, no. 4, pp. 358–363, 2006.
[28] T. Mimler et al., "Extracellular matrix in ascending aortic aneurysms and dissections–What we learn from decellularization and scanning electron microscopy," *Plos One*, vol. 14, no. 3, 2019, Art. no. e0213794.
[29] K. M. Saqr et al., "What does computational fluid dynamics tell us about intracranial aneurysms? A meta-analysis and critical review," *J. Cerebr. Blood Flow Metabol.*, vol. 40, no. 5, pp. 1021–1039, 2020.
[30] G. Soulat et al., "4D Flow with MRI," *Annu. Rev. Biomed. Eng.*, vol. 22, pp. 103–126, Jun. 2020.
[31] J. J. Chiu and S. Chien, "Effects of disturbed flow on vascular endothelium: Pathophysiological basis and clinical perspectives," *Physiol. Rev.*, vol. 91, no. 1, pp. 327–387, 2011.
[32] D. N. Ku et al., "Pulsatile flow and atherosclerosis in the human carotid bifurcation. Positive correlation between plaque location and low oscillating shear stress," *Arterioscler. Thromb. Vasc. Biol.*, vol. 5, no. 3, pp. 293–302, 1985.
[33] R. Trip et al., "An experimental study of transitional pulsatile pipe flow," *Phys. Fluid*, vol. 24, no. 1, 2012, Art. no. 014103.